Available online at www.sciencedirect.com
ScienceDirect
Journal of Catalysis 251 (2007) 213–222
JOURNAL OF CATALYSIS
www.elsevier.com/locate/jcat

Structured catalyst of Pd/ZnO on sintered metal fibers for 2-methyl-3-butyn-2-ol selective hydrogenation

Natalia Semagina [a], Martin Grasemann [a], Nicolas Xanthopoulos [b], Albert Renken [a], Lioubov Kiwi-Minsker [a,*]

[a] *Group of Chemical Reaction Engineering, Ecole Polytechnique Fédérale de Lausanne, GGRC-EPFL, Station 6, CH-1015 Lausanne, Switzerland*
[b] *Metallurgical Chemistry Laboratory, EPFL-STI-IMX-LMCH, Station 12, CH-1015 Lausanne, Switzerland*

Received 27 April 2007; revised 24 June 2007; accepted 27 June 2007

Available online 23 August 2007

Abstract

An innovative structured catalyst based on sintered metal fibers (SMFs) coated by a grain-structured ZnO layer was developed for the selective 3-phase hydrogenation of functionalized alkynes. The catalyst was synthesized by the deposition of Pd^0-sol with 7-nm nanoparticles stabilized by molybdate anions on ZnO/SMF after reduction in hydrogen at 773 K. The crystallites of PdZn alloy (24 nm) were formed by high-temperature treatment in hydrogen and contained partly Pd(0) nanoparticles. Pd/ZnO/SMF (0.2 wt% Pd, 6 wt% ZnO) allowed >95% yield of 2-methyl-3-buten-2-ol (MBE) during 2-methyl-3-butyn-2-ol hydrogenation at 308 K and 5 bar pressure using water as the solvent and adding a small amount of quinoline. The consecutive reaction of MBE hydrogenation was suppressed due to the presence of PdZn in the active phase. The catalyst activity of the catalyst was an order of magnitude higher compared with that of commercial Lindlar catalyst (Pd, Pb/$CaCO_3$), which quickly deactivated in aqueous media due to irreversible chemical transformations of the $CaCO_3$ support. The structured catalyst developed in this study could be reused after ultrasonic regeneration, retaining the original selectivity and most of its initial activity. The catalyst showed high mechanical stability, precluding leaching of its components during the reaction. Due to easy shaping, high permeability, and low pressure drop during the fluid passage, the structured Pd/ZnO/SMF catalyst is suitable for a continuously operated staged bubble column reactor.

Keywords: Palladium; Sintered metal fiber; Structured catalyst; Hydrogenation; Acetylene alcohol; 2-methyl-3-butyn-2-ol; Quinoline; Ultrasonic regeneration

1. Introduction

Pd-catalyzed three-phase hydrogenation of functionalized alkynes to alkenes is important in fine chemical production [1,2]. Conventionally, the reactions are carried out in semi-batch slurry reactors using a powdered Lindlar catalyst, 5% Pd/$CaCO_3$, modified by lead acetate [3]. The Lindlar catalyst allows a high product yield but deactivates after the first run if water is used as a solvent, and it must be separated from the reaction products. A quest for hydrogenation process intensification implies the need for a rational reactor design suitable for continuous operation and the development of an appropriate structured catalyst.

Over the last decade, structured catalysts have attracted increasing attention for three-phase reactions [4–15]. Palladium catalysts based on monoliths [7,8], H_2-permeable membranes [9,10], metallic grids [11,12], and bidimensional glass [13] and carbon [14,15] fabrics have shown high selectivity to alkenes in liquid-phase hydrogenation. The disadvantages of these structured catalysts are low surface area, low reactor space–time yield, high fabrication costs, or low mechanical strength. Pd-loaded fabrics of activated carbon fibers were recently proposed by us for 2-butyne-1,4-diol hydrogenation in a bubble column [15], but they required the placement of supporting metallic grids in a staged bubble column reactor (SBCR). The SBCR has been designed for continuous operation of multiphase reactions with increased efficiency, providing high productivity per reactor volume. The low liquid holdup is an additional advantage of SBCR due to safety concerns.

* Corresponding author.
E-mail address: lioubov.kiwi-minsker@epfl.ch (L. Kiwi-Minsker).

0021-9517/$ – see front matter
doi:10.1016/j.jcat.2007.06.028

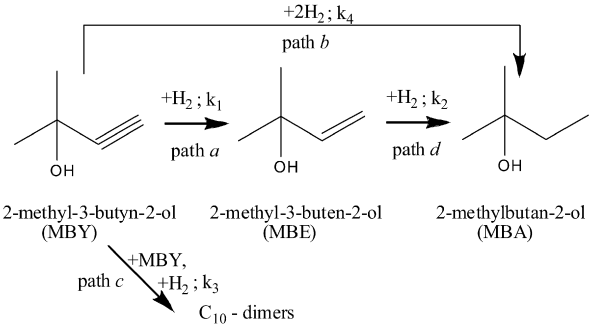

Fig. 1. Reaction scheme of 2-methyl-3-butyn-2-ol (MBY) hydrogenation with the corresponding rate constants k_i.

In this work, we chose three-dimensional sintered metal fibers (SMFs) as a structured support for the active phase. The SMF sheets have high permeability, good mechanical strength, and high thermal conductivity, making them advantageous for exothermic hydrogenation [16–22]. They can be easily shaped and placed in SBCR. The metal fiber matrix also acts as a microscale static mixer, preventing channeling [19] and improving mass transfer. Coating the fiber surface with a thin, catalytically active layer (∼10% of a microfiber diameter) has been reported to not affect its permeability, and the pressure drop remains low during fluid passage through the catalytic bed [18,20,21,23].

The goal of the present work was to develop a structured SMF-based catalyst that is active/selective in the hydrogenation of an acetylenic alcohol in aqueous media and provides a valuable alternative to commercial Lindlar catalyst (powder of Pd, $Pb/CaCO_3$). The latter is known to be not suitable for hydrogenation in aqueous media due to irreversible deactivation caused by the support hydroxylation. For the first time, SMF-based catalysts were applied for three-phase hydrogenations. As a model reaction, the hydrogenation of 2-methyl-3-butyn-2-ol (MBY) to 2-methyl-3-buten-2-ol (MBE, Fig. 1) with a water as solvent was studied. MBE is an important intermediate in the synthesis of vitamins (A, E) and perfumes [24]. Pd-based catalysts are known to give the highest selectivity and yield of alkenols [14,25–30]. The MBY hydrogenation reaction is structure-sensitive; Pd/Al_2O_3 catalyst with monodispersed 2.5-nm particles showed sixfold lower activity and lower selectivity (75 vs 89%) compared with Pd/Al_2O_3 containing monodispersed 7.5-nm particles [31]. The performance of Pd catalyst in alkynol hydrogenation is strongly influenced not only by the Pd dispersion [31,32], but also by the nature of the support [28,33], the promoters to active metals [3,9,34–44], and use of additives [7,45–48]. For MBY hydrogenation in ethanol as solvent, selectivity to MBE has been found to increase in the following order: Pd black < Pd/C < Pd/Al_2O_3 < $Pd/BaSO_4$ < Pd/MgO < Pd/ZnO ≅ $Pd/CaCO_3$ [33]. The ZnO is the support of choice, because zinc also acts as a promoter [39–44]. Promoters are known to affect the adsorption of alkynols and alkenols on Pd nanoparticles and to suppress the formation of β-PdH phase, responsible for the direct alkynol hydrogenation to saturated alcohol [49]. To date, only Pd/ZnO powder has been reported as a catalyst for 3-phase alkyne hydrogenations, and no data on the catalyst reuse in aqueous media have been reported.

Proper design of a SBCR requires data on catalyst activity, selectivity, and stability. Because the testing of a structured catalyst is usually performed in a batch regimen [7], we used a semibatch reactor to carry out MBY hydrogenation with the developed catalyst. This catalyst could be reused in consecutive runs without filtration. A rational synthetic procedure applied for the SMF coating led to the active/selective catalytic phase of Pd/PdZn/ZnO with improved stability in aqueous media compared with the commercial Lindlar catalyst. The nature of the active phase was explored. The catalysts were characterized by SEM, XRD, XPS, BET, CO chemisorptions analysis, and adherence tests. The reaction kinetics were studied; we found that the model based on the Langmuir–Hinshelwood mechanism is consistent with the experimental data.

2. Experimental

2.1. Materials

SMFs (Southwest Screens & Filters SA, Belgium) made of FeCrAl alloy fibers (Cr 20%, Al 4.75%, Y 0.27%, other elements ∼1–2%, Fe balance) in the form of a uniform pore panel (0.29 mm thickness, 71% porosity, 20 μm fiber thickness, 675 g/m^2) [20] were used as a structured support.

Zinc acetate dihydrate (puriss. p.a., ⩾99.5%), monoethanolamine (ethanolamine, puriss. p.a., ⩾99%), acetoin (3-hydroxy-2-butanone, purum, mixture of monomer and dimer), sodium molybdate dihydrate (puriss. p.a., >99%), palladium(II) chloride anhydrous (purum), powdered zinc oxide (purum, p.a.), nitric acid (puriss., p.a.), ethanol (purum, ⩾99.8%), toluene (puriss. p.a., ⩾99.7%), and 2-propanol (puriss. p.a., >99.8%) were supplied by Fluka. Acetone (puriss., >99%) was purchased from Riedel–de Haen. Powdered ZnO was calcined before use at 693 K for 3 h. Lindlar catalyst (5 wt% Pd and 3.5 wt% Pb content, as confirmed by atomic absorption spectroscopy [AAS]), a commercially available sample, was stored under ambient conditions and used as received.

2-Methyl-3-butyn-2-ol (purum, ⩾99%), 2-methyl-3-buten-2-ol (purum, ⩾97%), 2-methyl-2-butanol (purum, ⩾98%), 1-butanol (purum, ⩾99.5%), and quinoline (purum, ⩾97%) were purchased from Fluka and used as received. Hydrogen (⩾99.99% purity) was obtained from Carbagas, Switzerland. Bidistilled water was used throughout this work.

2.2. Preparation of Pd/ZnO/SMF catalyst (0.2 wt% Pd {3 wt% to ZnO}, 6 wt% ZnO)

To remove contamination, the SMF panels were degreased with acetone, boiled in toluene for 0.5 h, and air-dried. To further improve adhesion of ZnO, the SMFs were oxidized in air at 1373 K for 3 h to create an α-Al_2O_3 surface layer. Such a temperature (1373–1473 K) for the treatment of FeCrAl alloy with a low rare earth content is known to lead to the formation of a structured alumina film, characterized by equiaxed grains on the outer surface, whereas a lower-temperature treatment yields oxide whiskers [50,51].

ZnO film was prepared by the sol–gel method [52] using zinc acetate dihydrate (0.3 M in isopropanol) and solubility enhancement additives monoethanolamine (MEA) and acetoin (AIN) at a molar ratio of MEA:AIN:Zn = 1:0.5:1. The additives were mixed in a solvent before the addition of zinc acetate with the help of ultrasound, the sol was a reddish-brown color due to the reaction between MEA and AIN, yielding imine HO–$CH(CH_3)$–$C(CH_3)$=N–C_2H_4–OH [53]. Coating was done by a dip-coating procedure. The gel film thus obtained was air-dried at 383 K for 10 min and then heated at 873 K for 30 min [54]. Rapid heating was applied, which is known to result in the formation of highly oriented crystals, whereas slow heating is known to give plicated structures [55]. The coating-heating procedure was repeated 7 times to deposit ∼6 wt% ZnO. The coating then was postannealed at 1173 K for 15 min to promote the formation of island structure of ZnO grains with increased specific surface area [55].

Pd sol was prepared via dissolution of $PdCl_2$ in a boiling aqueous solution of sodium molybdate at a molar ratio Mo:Pd = 1.2, followed by hydrogenation for 30 min at room temperature [56]. This procedure is known to lead to Pd nanoparticles of 3–8 nm, which is the optimal size for structure-sensitive MBY hydrogenation [31]. After wet impregnation for 1 h, ZnO/SMF panels were washed copiously with water, dried at ambient conditions, and subjected to high-temperature treatment in hydrogen atmosphere (H_2:Ar = 1:9, total flow of 450 ml/mn, 2 h at room temperature, 10°/min to 773 K, hold for 2 h, and cooled at the same flow). The catalyst was stored at ambient conditions and used within 2 weeks after preparation ("fresh catalyst"). It was tested also after 2-month storage ("aged catalyst").

For comparison, Pd/ZnO/SMF (0.1 wt% Pd) was also synthesized via impregnation of ZnO/SMF with aqueous solution of Na_2PdCl_4, followed by reduction in hydrogen flow at 773 K. Two powdered Pd/ZnO (6 wt% Pd) samples were prepared in the same manner as the structured catalyst using commercial ZnO. One of these samples was subjected to the high-temperature treatment in hydrogen, and the other was used in the noncalcined state. Pd/γ-Al_2O_3 (0.2 wt% Pd) was also synthesized from Pd sol and used without high-temperature treatment in hydrogen.

2.3. Catalyst characterization

The amounts of Pd and Zn after dissolution in hot nitric and hydrochloric acids were determined by AAS using a Shimadzu AA-6650 spectrometer with an air-acetylene flame. ZnO loading was also determined gravimetrically. The BET specific surface area and pore size distribution (PSD) of the support and the catalyst were determined using a Sorptomatic 1990 (Carlo Erba) instrument via N_2 adsorption–desorption at 77 K. PSD calculation was performed using the Dollimore/Heal method [57]. The surface morphology of the samples was investigated by scanning electron microscopy (SEM) using a JEOL JSM-6300F instrument.

The ultrasonic adherence test for the mechanical stability of the catalyst was carried out using a Bransonic ultrasonic cleaner (Branson Ultrasonic Corp.) [58]. The catalyst was ultrasonically treated in water for 20 min; every 5 min, it was dried at 393 K and weighed. XRD analysis was done in a Siemens D 500 diffractometer using Cu$K\alpha$ radiation. The spectra of Pd/ZnO/SMF samples were recorded in a rapid scanning mode (4.0 s/step, 2θ step size of 0.04°) in a 2θ range of 30°–50°. XRD spectra were also recorded at 2θ of 35°–90° for the powdered 6% Pd/ZnO sample. Scherrer's equation was used to calculate the Pd and PdZn particle sizes.

XPS of the powdered 6% Pd/ZnO samples was performed using an Axis Ultra ESCA system (Kratos, Manchester, UK) with monochromated Al$K\alpha$ radiation (1486.6 eV) and an X-ray power of 150 W. The binding energy (BE) values were referenced against a C 1s = 285.0 eV line. Standard pretreatment in vacuum was applied for 2 h. Because heating in vacuum could provide PdZn-phase formation, this was avoided. Samples were analyzed within a week after preparation.

Pd dispersion of the Lindlar catalyst was measured by pulse adsorption of CO (3% CO in He) carried out at 323 K in an Micromeritics AutoChem 2910. Before the measurements, the catalyst was pretreated at 353 K in flows of He (10 ml/min, STP), H_2 (20 ml/min, STP), and He (10 ml/min, STP). A stoichiometry of CO/Pd = 0.6 and a Pd surface density of 1.2×10^{19} atoms/m^2 were used for these calculations.

2.4. Hydrogenation experiments

Hydrogenations were carried out in a semibatch stainless steel reactor (250 ml autoclave; Buchi AG, Uster, Switzerland) equipped with a heating jacket and a hydrogen supply system. An autoclave was used for the catalytic performance test in three-phase reactions [7,14]. The structured catalyst was placed between two metal gauzes (2 × 8.5 cm) fixed on the self-gassing hollow shaft stirrer. The reaction with the Lindlar catalyst was carried out using an 8-blade disk turbine impeller. At the working temperature, the reactor was filled with the reaction mixture and the catalyst, flushed with N_2, and kept for 5 min under stirring to equalize the temperature. Then the reactor was flushed with hydrogen and pressurized. The pressure in the reactor was kept constant during the course of the reaction.

The experiments were carried out at 308 K and 5 bar H_2 pressure under intensive stirring at 2000 rpm. Bidistilled water containing 0.1 M of 2-methyl-3-butyn-2-ol in a total volume of 200 ml was used as the reaction medium. For both the structured and Lindlar catalysts, 0.9 mg of Pd was used, giving a substrate-to-palladium molar ratio of 2400. In some experiments, quinoline was added to the reaction medium.

The samples of the reaction mixtures were periodically withdrawn from the reactor via a sampling tube and analyzed by gas chromatography (GC) using a Perkin–Elmer Auto System XL equipped with a 30-m Stabilwax Crossbond Carbowax-PEG (Restek) 0.32-mm capillary column with a 0.25-μ coating. The carrier gas (He) pressure was 101 kPa. The injector and flame ionization detector temperatures were 473 and 523 K, respectively. The oven temperature was maintain for 4 min at 323 K, then increased to 473 K at a ramp of 30°/min. The GC analysis also allowed detection of the dimerized byproducts formed

during the reaction. 1-Butanol was used as an internal standard (0.74 g), allowing determination of the actual quantity of the reaction mixture components. The average molar weight of the dimers was assumed to be 168 g/mol. Yield to a product i (i = MBE, MBA, or dimers) was defined as $Y_i = [\text{mol}_{\text{MBY}}\ (\text{converted into } i)/\text{mol}_{\text{MBY}}\ (\text{introduced})] \times 100\%$, MBY conversion as $X = [\text{mol}_{\text{MBY}}\ (\text{reacted})/\text{mol}_{\text{MBY}}\ (\text{introduced})] \times 100\%$, and the selectivity was defined as $S_i = [Y_i/X] \times 100\%$ [59].

To estimate a standard deviation, six identical experiments were carried out. Error of the activity determination was about 3%. Standard deviations were ±0.1% in MBE and MBA selectivities and ±0.02% in dimer selectivity.

2.5. Catalyst reuse and regeneration

Between the hydrogenation runs, the structured catalyst was washed with water, dried at ambient conditions, and stored in vacuum desiccator. Two regeneration procedures were applied: (1) calcination at 773 K for 2 h with subsequent reduction in hydrogen atmosphere at 773 K for 2 h as described in Section 2.2, and (2) placing the catalyst in a beaker with ethanol, ultrasonically treating it for 10 min in the ultrasonic bath, and washing with water. The Lindlar catalyst was filtrated from the reaction mixture, washed with water, and dried at 323 K.

3. Results and discussion

3.1. Characterization of Lindlar and Pd/ZnO/SMF catalysts

According to the SEM analysis, the Lindlar catalyst contains 1.5 × 0.5 μm needles agglomerated in the hedgehog-like ∼10 μm formations. BET specific surface area was found to be 11 m^2/g. Quantitative surface composition was revealed by XPS analysis showing 18% Pd, 12% C, 17% Ca, 36% O, and 17% Pb (in weight %); 77% of the surface Pd was in its metallic form Pd^0 ($3d_{5/2}$ BE of 335.1 eV), along with 16% of Pd^{2+} assigned to PdO (BE of 336.3 eV) and 7% of Pd^{4+} assigned to PdO_2 (BE of 337.7 eV). Three types of surface Pb species were revealed by XPS: 24% Pb(0) with a $4f_{7/2}$ BE of 136.9 eV, 53% Pb^{2+} of PbO (BE = 139.3 eV), and 23% Pb^{2+} of $PbCO_3$ (BE = 138.3 eV). X-rays showed the calcite and aragonite as crystalline phases of $CaCO_3$, cerussite ($PbCO_3$), PbO, hydrate of PbO, and metallic Pd as Pd(111) and Pd(200) crystallites. CO chemisorption indicated a low Pd dispersion (2.5%).

BET specific surface area of the synthesized Pd/ZnO/SMF material was found to be ∼0.7 m^2/g, with a pore specific volume of 6×10^{-3} cm^3/g and mean pore radius of 1.2 nm. These values are in agreement with the surface areas of SMF (<1 m^2/g) [20] and ZnO powder (4 m^2/g) [60].

SEM microphotographs of the calcined SMF, SMF coated by ZnO (ZnO/SMF), and Pd/ZnO/SMF sheets are presented in Figs. 2a–2c. The calcined SMF microfibers (∼22 μm diameter) were fully coated with the grain-structured ZnO layer (∼1.5 μm thick), which remains intact after Pd deposition and high-temperature treatment. Neither detached ZnO grains nor large aggregates at the points of fibers contact were observed in the coated samples. Coating SMFs with a thin catalytically active layer preserves the advantages of this 3D material, especially in terms of its high permeability and low pressure drop during the fluid passage [18,20,21].

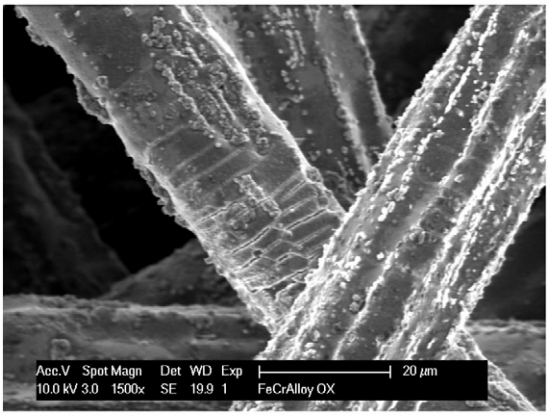

(a)

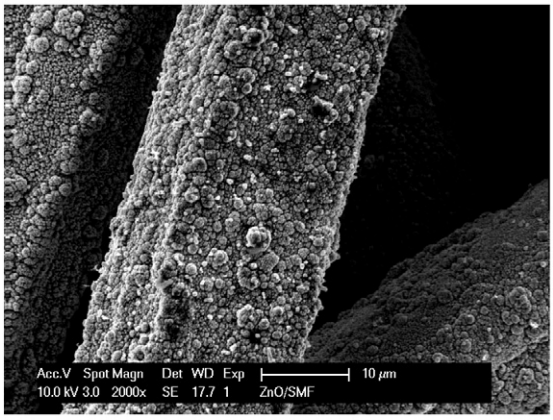

(b)

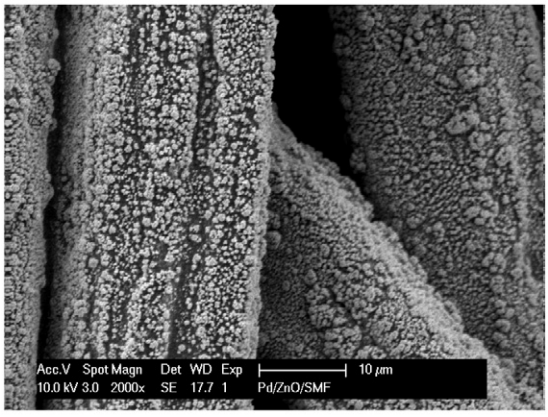

(c)

Fig. 2. SEM microphotographs of the (a) calcined SMF, (b) 6 wt% ZnO/SMF, and (c) 0.2 wt% Pd/6 wt% ZnO/SMF materials.

The adherence test for mechanical stability of the ZnO layer was performed using ultrasonic treatment of the ZnO/SMF in water. Cumulative weight loss of ZnO after 20 min of treatment was 0.25 wt% with respect to ZnO weight. Thus, the structured ZnO/SMF material has high mechanical stability and resistance in water media. This high adherence may be attributed to the formation of a thin layer of mixed oxides between FeCrAl alloy

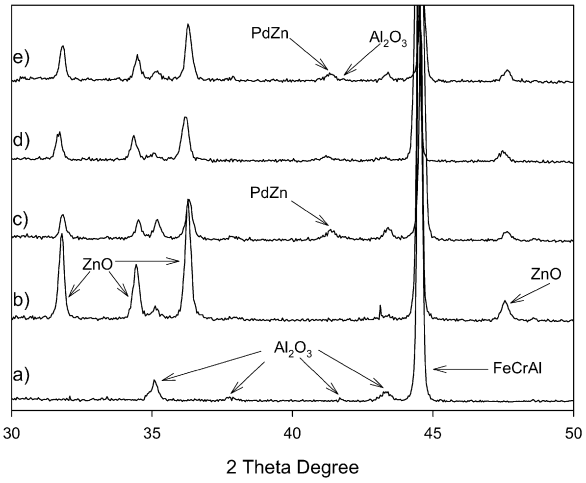

Fig. 3. XRD patterns of the (a) calcined SMF, (b) 6 wt% ZnO/SMF, and 0.2 wt% Pd/6 wt% ZnO/SMF: (c) fresh, (d) aged, (e) aged catalyst regenerated via calcination–reduction as described in Section 2.5.

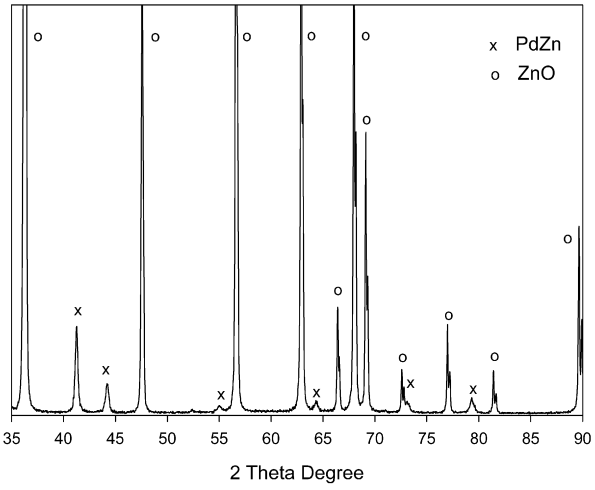

Fig. 4. XRD pattern of 6 wt% Pd/ZnO.

and ZnO at 1173 K, like $ZnAl_2O_4$ [61] or $ZnFe_2O_4$ [62]. Oxide layer formation also has been reported for ZnO-coated ZrO_2 [52] and SiO_2 [55].

XRD patterns of the calcined SMF, ZnO/SMF, and Pd/ZnO/SMF materials are shown in Figs. 3a–3c. Calcination of FeCrAl alloy SMF filters resulted in the formation of the surface alumina layer, in agreement with previously reported data [50,51]. Characteristic peaks of crystalline ZnO appeared in the samples, due to oxide formation by a sol–gel method. Deposited Pd nanoparticles had an average size of 7 nm as determined by XRD of powdered Pd/ZnO sample before high-temperature treatment in hydrogen atmosphere. After the treatment, characteristic peaks of palladium were no longer present in an XRD pattern. At the same time, peaks at 2θ of 41.2°, 44.1°, 54.4°, 64.2°, 72.7°, 79.2°, and 89.0° were found (Fig. 4), which are characteristic of the PdZn alloy. It is known that high-temperature reduction of Pd supported on ZnO induces strong metal–support interaction and the formation of PdZn intermediates [60,63–66]. Average PdZn particle size calculated from Scherrer's equation was found to be 24 ± 1 nm for both the powdered Pd/ZnO (Fig. 4) and the structured Pd/ZnO/SMF (Fig. 3c) catalysts.

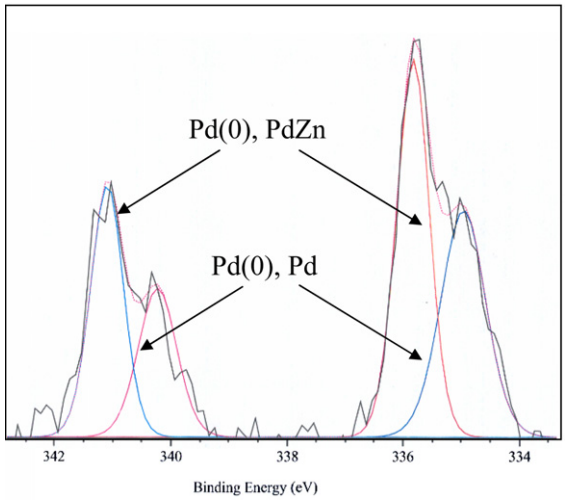

Fig. 5. XPS of the Pd 3d region of 6 wt% Pd/ZnO.

An XPS spectrum of the Pd 3d region (Pd $3d_{5/2}$ and Pd $3d_{3/2}$) of the Pd/ZnO powder treated at high temperature is shown in Fig. 5, along with the deconvolved peaks. Two types of Pd species were observed. The first of these, with BE of 335.0 eV, is assigned to Pd(0), and the other one has a BE of 335.8 eV. It is known [65,67] that in the presence of ZnO (or in the PdZn phase), the Pd $3d_{5/2}$ BE of Pd(0) shifts to higher values by 0.8 eV [67] or 0.6 eV. This result is in agreement with the mechanism of PdZn-phase formation [63]; at 773 K in hydrogen atmosphere and in the presence of Pd(0), ZnO is easily reduced and forms a Pd–Zn alloy of 24 ± 1 nm with a "flying saucer" shape, as calculated from XRD. The main part of the "flying saucer" consists of PdZn alloy containing some of the initial Pd^0 nanoparticle [63]. Determining the size of the Pd nanoparticles is impossible, because the nanoparticles are incorporated within the PdZn crystallites.

XPS analysis of a Pd/ZnO powder before the high-temperature treatment in hydrogen identified the molybdenum species responsible for Pd nanoparticle stabilization. XPS revealed no PdO, Cl from Pd precursor, or Na from sodium molybdate. A Mo:Pd molar ratio of 1:2 was used for the Pd sol during catalyst preparation, but this ratio decreased to 0.7 in the resulting catalyst. It is likely that the excess of molybdenum, which did not participate in the stabilization of Pd nanoparticles, was washed out during the catalyst preparation. A Mo 3d BE of 232.9 eV was assigned to MoO_x mixed oxide species. Considering the Paneth–Fajans rule, Pd nanoparticles are positively charged due to Pd^{2+} ions constituting a growing particle. Molybdate ions are charged negatively and provide electrostatic stabilization of the Pd nanoparticles. ZnO, being a basic support with an IEP of 8.7–9.7, is positively charged in distilled water at pH $\sim$ 6 and can efficiently adsorb Pd nanoparticles with a negative diffusion layer.

Thus, Pd^0 nanoparticles of 7 nm were prepared via electrostatic stabilization by molybdenum species and adsorbed on the ZnO/SMF surface. On treatment in hydrogen at 773 K, a PdZn alloy was formed, and Pd^0 was still present as part of the

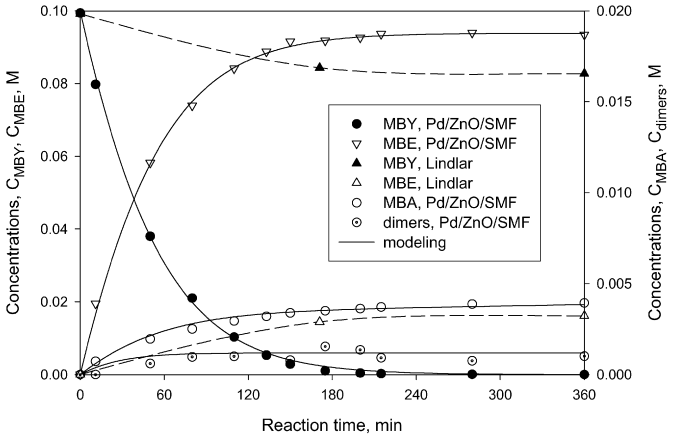

Fig. 6. Concentrations of MBY and products vs reaction time during hydrogenation over 0.2 wt% Pd/6 wt% ZnO/SMF catalyst. Reaction conditions: 0.1 M MBY in water, reaction volume of 200 ml, 0.9 mg Pd, 308 K, 5 bar, stirring rate of 2000 rpm.

Pd/PdZn crystallites with size of ∼24 nm. The structured catalyst showed high mechanical stability and precluded leaching in water.

3.2. Catalytic performance of Pd/ZnO/SMF catalyst with and without quinoline addition

Catalytic performance of the structured Pd/ZnO/SMF material was compared with that of the Lindlar catalyst. The maximum MBE yield for the Pd/ZnO/SMF catalyst was 94.5% at 99.9% MBY conversion. Concentration profiles of MBY and products versus reaction time are presented in Fig. 6 for fresh SMF-based and Lindlar catalysts at the same Pd loading in the reactor. For Pd/ZnO/SMF, the MBY concentration decreased concomitant with the increase in MBE concentration. Dimer formation stopped when all MBY was consumed, as has been reported for MBY hydrogenation [68]. MBA appeared at the very beginning of the reaction, confirming the presence of a parallel path b (Fig. 1) for direct MBY hydrogenation to MBA. This is usually observed during MBY hydrogenation over Pd catalysts [68]. Direct alkane formation from alkyne may proceed via ethylidyne species, as was shown by ^{14}C labeling in acetylene/ethylene hydrogenation experiments [69]. Once MBY is consumed, the rate of MBA formation drops to zero. Therefore, for the MBY hydrogenation over Pd/ZnO/SMF catalyst, the path d of MBE hydrogenation to MBA is suppressed, in contrast to the situation over monometallic Pd and Pd/Pb-containing catalysts [68].

TOF in MBY hydrogenation shows an antipathetic structure sensitivity [68]. Pd nanoparticles >6 nm are more active and also have >89% selectivity to MBE, whereas 2.5-nm particles exhibit only 75% selectivity to MBE [31,68]. High selectivity of the synthesized catalyst is due to the high activity for path a (see the reaction scheme in Fig. 1); therefore, its high performance is due mainly to the optimal size of Pd nanoparticles (7 nm before high-temperature treatment) provided by stabilization with molybdenum species. When Pd/ZnO/SMF catalyst was synthesized not from Pd sol, but rather through impregnation with Na_2PdCl_4 followed by reduction in hydrogen, its activity was an order of magnitude lower than that of the catalyst from Pd sol. This can be attributed to the smaller Pd nanoparticles involved in PdZn-phase formation.

Molybdenum is also known to decrease hydrogen and olefin adsorption strength on Pt group metals, thus influencing the selectivity and activity of hydrogenation reactions [70]. However, in the present study, it was not possible to distinguish between this effect and the size sensitivity of MBY hydrogenation. Mo-stabilized Pd nanoparticles were also deposited on Al_2O_3 and ZnO without treatment at high temperature. The Pd/Al_2O_3 catalyst exhibited 2% lower selectivity but threefold higher activity than Pd/ZnO. PdZn phase was detected by XPS also in the non-treated sample at ambient conditions [41,64]. Despite the high activity for path a, both catalysts did not suppress path d, but the rate of MBE hydrogenation was lower for Pd/ZnO than for Pd/Al_2O_3. This can be rationalized by the presence of the PdZn phase; path d was suppressed more at a higher content of PdZn phase. The PdZn phase is known to provide a high selectivity to MBE [41,60,64].

The reaction carried out under similar conditions with the same Pd loading using the commercial Lindlar catalyst showed an order-of-magnitude lower initial activity of 0.04 $mol_{MBY}/mol_{Pd}/s$ compared with the 0.71 $mol_{MBY}/mol_{Pd}/s$ of the Pd/ZnO/SMF catalyst, and it deactivated in aqueous media. Water is known to deactivate the Lindlar catalyst due to changes in the catalyst's chemical and morphological structures [34]. In contrast, Pd/ZnO/SMF is stable in water and thus represents an excellent alternative to the Lindlar catalyst for hydrogenation in aqueous media.

Fig. 6 also shows the simulated kinetic curves for hydrogenation over Pd/ZnO/SMF catalyst obtained on the base of a Langmuir–Hinshelwood model assuming competitive adsorption of the reactants on one type of active site and bimolecular reactions of the adsorbed species. To comply with the conditions of the first order to hydrogen and its known dissociative adsorption on Pt group metals, addition of the second hydrogen atom to the adsorbed organic species is considered the rate-determining step, whereas addition of the first atom is quasi-equilibrated [71,72]. The transformation rate of MBY to MBE can be expressed as

$$r_1 = k_1^* K_{MBY} C_{MBY} \big(1 + K_{MBY} C_{MBY} + K_H^{1/2} C_{H_2}^{1/2} + K_{MBE} C_{MBE} + K_{MBA} C_{MBA} + K_{dimers} C_{dimers}\big)^{-1/2}, \quad (1)$$

where $k_1^* = k_1 K_{MBY\text{-}H} C_{H_2} K_H$, k_1 is a reaction rate constant, and K_{MBY}, K_{MBE}, K_{MBA}, K_{dimers}, K_H, and K_{MBY-H} are the adsorption equilibrium constants of MBY, MBE, MBA, dimers, a hydrogen atom, and a half-hydrogenated MBY. Because the adsorption equilibrium constants of the products are small compared with the adsorption constant of the acetylenic reactant, it can be assumed that $K_{MBE} \cong K_{MBA} \cong K_{dimers}$, thus reducing the number of adjustable model parameters. Also taking into consideration the weak hydrogen adsorption on Pt group metals [71], $K_{H_2} \ll 1$, Eq. (1) may be simplified as

$$r_1 = k_1^* K_{\mathrm{MBY}} C_{\mathrm{MBY}} \big(1 + K_{\mathrm{MBY}} C_{\mathrm{MBY}} + K_{\mathrm{MBE}}(C_{\mathrm{MBE}} + C_{\mathrm{MBA}} + C_{\mathrm{dimers}})\big)^{-1/2}. \quad (2)$$

For MBE transformation to MBA and MBY to dimers, the expressions can be developed:

$$r_2 = k_2^* K_{\mathrm{MBE}} C_{\mathrm{MBE}} \big(1 + K_{\mathrm{MBY}} C_{\mathrm{MBY}} + K_{\mathrm{MBE}}(C_{\mathrm{MBE}} + C_{\mathrm{MBA}} + C_{\mathrm{dimers}})\big)^{-1/2} \quad (3)$$

and

$$r_3 = k_3^* K_{\mathrm{MBY}}^2 C_{\mathrm{MBY}}^2 \big(1 + K_{\mathrm{MBY}} C_{\mathrm{MBY}} + K_{\mathrm{MBE}}(C_{\mathrm{MBE}} + C_{\mathrm{MBA}} + C_{\mathrm{dimers}})\big)^{-1/2}. \quad (4)$$

Direct hydrogenation of MBY to MBA is assumed to proceed via two bimolecular elementary steps without desorption of the adsorbed intermediate MBE [27],

$$r_4 = k_4^* K_{\mathrm{MBY}} C_{\mathrm{MBY}} \big(1 + K_{\mathrm{MBY}} C_{\mathrm{MBY}} + K_{\mathrm{MBE}}(C_{\mathrm{MBE}} + C_{\mathrm{MBA}} + C_{\mathrm{dimers}})\big)^{-1/2}. \quad (5)$$

The mass balances for MBY and the reaction products are given by the following differential equations:

$$\frac{dC_{\mathrm{MBY}}}{dt} = -\frac{m_{\mathrm{cat}}}{V_{\mathrm{L}}}(r_1 + 2r_3 + r_4), \quad (6)$$

$$\frac{dC_{\mathrm{MBE}}}{dt} = \frac{m_{\mathrm{cat}}}{V_{\mathrm{L}}}(r_1 - r_2), \quad (7)$$

$$\frac{dC_{\mathrm{MBA}}}{dt} = \frac{m_{\mathrm{cat}}}{V_{\mathrm{L}}}(r_2 + r_4), \quad (8)$$

and

$$\frac{dC_{\mathrm{dimers}}}{dt} = \frac{m_{\mathrm{cat}}}{V_{\mathrm{L}}} r_3, \quad (9)$$

where m_{cat} is the catalyst mass and V_{L} is a volume of liquid phase in the reactor.

Equations (6)–(9) were solved numerically with a Rosenbrock method using Madonna Berkeley software [73]. The model parameters were estimated by fitting the simulated curves to the experimental data (Fig. 6). Calculated model parameters were $K_{\mathrm{MBY}} = 1.9\ \mathrm{L\,mol^{-1}}$, $K_{\mathrm{MBE}} = K_{\mathrm{MBA}} = K_{\mathrm{dimers}} = 2 \times 10^{-3}\ \mathrm{L\,mol^{-1}}$, $k_1^* = 4.4 \times 10^{-2}\ \mathrm{mol\,g_{Pd}^{-1}\,s^{-1}}$, $k_2^* = 1.9 \times 10^{-2}\ \mathrm{mol\,g_{Pd}^{-1}\,s^{-1}}$, $k_3^* = 5.5 \times 10^{-3}\ \mathrm{mol\,g_{Pd}^{-1}\,s^{-1}}$, and $k_4^* = 1.6 \times 10^{-3}\ \mathrm{mol\,g_{Pd}^{-1}\,s^{-1}}$. The $K_{\mathrm{MBE}}/K_{\mathrm{MBY}}$ ratio was found to be 10^{-3}, explaining the suppression of MBE hydrogenation to MBA. For monometallic Pd catalysts, this ratio is 10^{-2}, decreasing in the presence of a promoter [27].

To improve the MBE yield in the hydrogenation with the structured catalyst, quinoline was added to the reaction mixtures. A nitrogen base (NB) is typically used in the concentrations, giving an NB/Pd molar ratio ranging from 4 to ∼1500 and an NB/substrate molar ratio of 0.1–1 [3,74–76]. In this work, quinoline was added in concentrations giving NB/Pd molar ratios of 480, 120, 26, and 7 and corresponding NB/substrate molar ratios of 0.2, 0.05, 0.01, and 0.0025. The results are summarized in Fig. 7 and Table 1. An increase in the NB/Pd ratio from 0 to 26 increased both the selectivity and the activity by 1%, and decreases the time needed to achieve 99.9% conversion by a factor of 6. Further increases in quinoline concentration lead to further improvements in selectivity, but the reactions are almost blocked at 98 and 73% conversion at Q/Pd = 120 and 480, respectively. The effect of the nitrogen organic bases is usually explained as (i) preferential adsorption of the additive over alkenol [45] (i.e., poisoning [site blocking] of the less selective sites [48]); (ii) decreased catalyst activity via unselective site blocking, which decreases the influence of mass-transfer limitations and leads to enhanced selectivity [7,45]; (iii) electron donation from the N-atom to Pd [29] and the change of the alkynol/alkenol relative adsorption strength ("ligand" effect) [28,74,75]; (iv) formation of $Pd^{\delta+}$–$H^{\delta-}$ mode on Pd surface resulting in nucleophilic H attack on the triple bond [46]; or (v) catalyst surface rearrangement [34]. Because the Pd/ZnO/SMF catalyst activity first increases and then drops with the addition of quinoline, we can attribute the activity increase to the "ligand" effect of the base and/or formation of $Pd^{\delta+}$–$H^{\delta-}$ mode on the Pd surface and attribute the activity decrease to the site-blocking effect at higher concentrations.

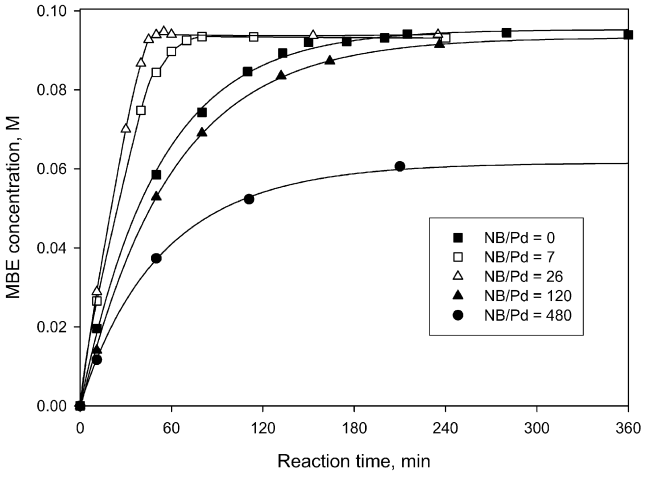

Fig. 7. MBE concentrations vs reaction time during hydrogenations over 0.2 wt% Pd/6 wt% ZnO/SMF with the use of quinoline at different nitrogen base/Pd (NB/Pd) molar ratio. For other reaction conditions see Fig. 6.

Table 1
Influence of quinoline (nitrogen base, NB) addition on the catalytic behavior of fresh Pd/ZnO/SMF (0.2 wt% Pd, 6 wt% ZnO). Reaction conditions, see Fig. 6

NB/Pd (mol/mol)	Initial activity ($\mathrm{mol_{MBY}/mol_{Pd}/s}$)	S_{MBE} at 99.9% conversion (%)	Time to 99.9% conversion (h)
0	0.7	94.5	4.7
7	1.0	94.3	1.3
26	1.1	95.5	0.8
120	0.5	97.0[a]	6.2[a]
480	0.4	97.0[b]	23[b]

[a] At 98% conversion as no further hydrogenation has occurred.
[b] At 73% conversion as no further hydrogenation has occurred.

Taken together, our findings indicate that the catalytic performance of the Pd/ZnO/SMF material is an order-of-magnitude greater than that of the Lindlar catalyst, This may be due to the presence of PdZn in the active catalytic phase, suppressing consecutive MBE hydrogenation to MBA.

Table 2
Performance of the aged and regenerated Pd/ZnO/SMF (0.2 wt% Pd, 6 wt% ZnO) catalyst in multiple runs (for the reaction conditions see Fig. 6, for the treatment conditions—Sections 2.2 and 2.5)

No.	Catalyst/reaction run	Initial activity ($mol_{MBY}/mol_{Pd}/s$)	S_{MBE} at 99.9% conversion (%)	S_{MBE}/S_{dimers} at 99.9% conversion (%)	Time to 99.9% conversion (h)
1	Fresh catalyst/run 1	0.71	94.5	1.7	4.7
2	Aged catalyst/run 1	0.83	93.5	2.0	2.9
3	Aged catalyst/run 3	0.68	90.0	2.1	1.9
4	Catalyst after No. 3 regenerated via calcination–reduction/run 1	0.36	91.5	0.8	6
5	Aged catalyst regenerated via calcination–reduction/run 1	0.66	93.0	0.8	7.5
6	Catalyst after No. 5 regenerated by ultrasound/run 1	0.43	94.6	1.0	10

3.3. Catalyst reuse

Due to the rigid open structure of SMFs with low pressure drop, the Pd/ZnO/SMF catalyst can be used as self-sustained catalytic stages in a bubble column reactor [15]. Before catalyst performance in a continuous mode is studied, catalyst stability at reuse and the possibility of regeneration should be investigated. Therefore, we reused the Pd/ZnO/SMF catalyst aged for 2 months at ambient conditions; the results are presented in Table 2. Both the Pd/ZnO/SMF and Lindlar catalysts were washed with water between the runs and dried in air. In the second run, the structured catalyst showed a 10% lower activity, whereas the Lindlar catalyst demonstrated no activity, due to its deactivation in aqueous media.

Zero leaching of Pd and <0.5 wt% leaching of Zn to the reaction mixtures were found via AAS. After storage, the catalyst showed higher activity (Table 2, Nos. 1 and 2), but the selectivity and yield of MBE decreased by 1% due to the increased formation of both MBA and dimers. XRD analysis of the aged catalyst (Fig. 3d) showed an approximate 50% decrease in the intensity of a PdZn peak at 2θ of 41.2°, which corresponds to a 60% increase in activity. As less Pd is involved in the PdZn phase, the activity increases [41,64]. The average PdZn crystallite size calculated by Scherrer's relation did not change compared with the crystallite size of the fresh catalyst of ∼23 nm. It is known that during storage, Pd/ZnO materials develop a more uniform distribution of the Pd and PdZn particles. This could be the reason for the activity increase observed in the structure-sensitive MBY hydrogenation [64].

Reuse of the aged catalyst with intermediate washing by water showed a progressive decrease in selectivity to MBE due to increased MBA and dimer formation (Table 2, Nos. 2 and 3). After 3 runs, the catalyst was regenerated by the calcination-reduction procedure (see Section 2.5), which in some cases is known to restore the initial catalytic performance of Pd catalysts in hydrogenation reactions [9]. However, the regeneration did not improve the selectivity significantly (Table 2, No. 4) and decreased the activity. Calcination–reduction treatment of Pd/ZnO catalysts is known to affect the state of metallic and bimetallic phases. During calcination, PdZn alloy is decomposed back to Pd crystallites and ZnO [63], which reform PdZn alloy during the subsequent reduction. To distinguish between these morphological changes and the removal of carbonaceous deposits during regeneration, the stored catalyst (as in No. 2 in Table 2) was subjected to the same calcination–reduction procedure. XRD analysis (Fig. 3e) again showed the presence of PdZn phase, but the selectivity and activity were lower than those of the fresh catalyst (Table 2, Nos. 1 and 5). The peak of the PdZn crystallite at 41.2° had ∼80% of the intensity of fresh catalyst. The average calculated size of crystallites was again found to be ∼24 nm. The lower activity is attributed to the formation of multiple intermediates under the calcination–reduction cycle, however, the characteristic peaks could not be detected, probably due to their very low intensity [64]. In both cases (Nos. 4 and 5), regeneration decreased the MBA formation, attaining the value observed for the fresh catalyst (Table 2, No. 1). However, the dimer formation increased, and the catalyst activity decreased.

No. 6 in Table 2 demonstrates the efficient catalyst regeneration via ultrasonic treatment in ethanol for 10 min. No Pd was detected in ethanol by AAS afterward. As can be seen, selectivity to MBE after the ultrasonic regeneration was fully restored to the level of the fresh catalyst; however, the activity decreased twice. The S_{MBA}/S_{dimers} ratio dropped from 2 to 1 after reuse and regeneration. Ultrasonic treatment is known to clean the surface of heterogeneous catalysts of carbonaceous deposits; it also provides morphological changes of the catalyst surface, allowing their reuse [77,78]. For comparison, the Lindlar catalyst was also subjected to the ultrasonic regeneration procedure; it exhibited no activity in the second run. This confirms that the cause of irreversible deactivation of the Lindlar catalyst was the chemical transformation of $CaCO_3$ support as a result of hydroxylation in aqueous media.

4. Conclusion

A new structured catalyst based on SMFs with high mechanical strength, high permeability, and low pressure drop has been developed for the 3-phase selective hydrogenation of functionalized alkynes. In contrast to the industrially used Lindlar catalyst, the new catalyst shows high activity, selectivity, and stability in aqueous media, as well as the possibility of reuse without the need for filtration. The catalyst was coated by a grain-structured ZnO layer and loaded with Pd^0-sol of 7-nm nanoparticles stabilized by molybdate anions. During the subsequent reduction in hydrogen at 773 K, 24-nm crystallites of Pd°/PdZn alloy were formed, as detected by XPS and XRD analyses. The phase Pd°/PdZn/ZnO was responsible for the catalyst activity/selectivity/stability during the hydrogenation in aqueous media.

Catalytic properties of Pd/ZnO/SMF (0.2 wt% Pd, 6 wt% ZnO) were tested in a semibatch hydrogenation of 2-methyl-3-butyn-2-ol in water to 2-methyl-3-buten-2-ol (MBE). The catalyst exhibited one-order-of-magnitude higher activity compared with the Lindlar catalyst and provided a 95.3% MBE yield at 308 K and 5 bar pressure in the presence of quinoline. The consecutive MBE hydrogenation to saturated alcohol was suppressed. The structured catalyst could be reused after ultrasonic regeneration, in contrast to the Lindlar catalyst, which deactivated completely in aqueous reaction media during the first run. Therefore, the Pd/ZnO/SMF catalyst seems to be suitable for continuously operated SBCR. This work is in progress and will be reported in future contributions.

Acknowledgments

Financial support was provided by the Swiss National Foundation and the Swiss Commission for Technology and Innovation. The authors thank M. Ruta for recording SEM images and E. Casali for the specific surface area measurements.

References

[1] B. Chen, U. Dingerdissen, J.G.E. Krauter, H.G.J.L. Rotgerink, K. Mobus, D.J. Ostgard, P. Panster, T.H. Riermeier, S. Seebald, T. Tacke, H. Trauthwein, Appl. Catal. A 280 (2005) 17.
[2] F. Roessler, Chimia 57 (2003) 791.
[3] H. Lindlar, Helv. Chim. Acta 35 (1952) 446.
[4] L. Kiwi-Minsker, Chimia 56 (2002) 143.
[5] Y. Matatov-Meytal, M. Sheintuch, Appl. Catal. A 231 (2002) 1.
[6] S. Irandoust, A. Cybulski, J.A. Moulijn, in: A. Cybulski, J.A. Moulijn (Eds.), Structured Catalysts and Reactors, Dekker, New York, 1998, p. 239.
[7] T.A. Nijhuis, G. van Koten, J.A. Moulijn, Appl. Catal. A 238 (2003) 259.
[8] J.M. Winterbottom, H. Marwan, E.H. Stitt, R. Natividad, Catal. Today 79 (2003) 391.
[9] A.N. Karavanov, V.M. Gryaznov, V.I. Lebedeva, I.A. Litvinov, A.Y. Vasilkov, A.Y. Olenin, Catal. Today 25 (1995) 447.
[10] V.M. Gryaznov, A.N. Karavanov, T.M. Belosljudova, A.V. Ermolaev, A.P. Maganjuk, I.K. Sarycheva, US patent 4,388,479, 1983.
[11] F.J. Broecker, L. Arnold, P. Grafen, US patent 5,063,194, 1991.
[12] J.P. Reymond, D. Dubois, P. Fouilloux, in: B. Delmon (Ed.), Preparation of Catalysts, vol. VII, Elsevier, New York, 1998, p. 63.
[13] V. Höller, K. Radevik, I. Yuranov, L. Kiwi-Minsker, A. Renken, Appl. Catal. B 32 (2001) 143.
[14] E. Joannet, C. Horny, L. Kiwi-Minsker, A. Renken, Chem. Eng. Sci. 57 (2002) 3453.
[15] L. Kiwi-Minsker, E. Joannet, A. Renken, Chem. Eng. Sci. 59 (2004) 4919.
[16] J. De Greef, G. Desmet, G. Baron, Catal. Today 105 (2005) 331.
[17] P. Tribolet, L. Kiwi-Minsker, Catal. Today 105 (2005) 337.
[18] I. Yuranov, A. Renken, L. Kiwi-Minsker, Appl. Catal. A 281 (2005) 55.
[19] D.R. Cahela, B.J. Tatarchuk, Catal. Today 69 (2001) 33.
[20] I. Yuranov, L. Kiwi-Minsker, A. Renken, Appl. Catal. B 43 (2003) 217.
[21] I. Cerri, M. Pavese, G. Saracco, V. Specchia, Catal. Today 83 (2003) 19.
[22] M.W. Meffert, Ph.D. thesis, Auburn University, Auburn, AL, 1998.
[23] V. Meille, Appl. Catal. A 315 (2006) 1.
[24] 3-buten-2-ol, 2-methyl, CAS N 115-18-4 UNEP Publications.
[25] H.-U. Blaser, A. Indolese, A. Schnyder, H. Steiner, M. Studer, J. Mol. Catal. A 173 (2001) 3.
[26] L. Cerveny, Chem. Eng. Commun. 83 (1989) 31.
[27] A. Molnar, A. Sarkany, M. Varga, J. Mol. Catal. A 173 (2001) 185.
[28] E.M. Sulman, Rus. Chem. Rev. 63 (1994) 923.
[29] T. Mallat, A. Baiker, Appl. Catal. A 200 (2000) 3.
[30] J.P. Boitiaux, J. Cosyns, E. Robert, Appl. Catal. 32 (1987) 145.
[31] N.A. Zakarina, G.D. Zakumbaeva, N.F. Toktabaeva, B.B. Dyusenbina, E.N. Litvyakova, A.S. Kuanyshev, Kinet. Catal. 24 (1983) 733.
[32] G.D. Zakumbaeva, N.A. Zakarina, V.A. Naidin, A.M. Dostiyarov, N.F. Toktabaeva, E.N. Litvyakova, Kinet. Catal. 24 (1983) 379.
[33] T.O. Omarkulov, Z. Mukataev, S.V. Goncharova, D.V. Sokol'skii, Rus. J. Phys. Chem. 59 (1985) 137.
[34] R. Schlogl, K. Noack, H. Zbinden, A. Reller, Helv. Chim. Acta 70 (1987) 627.
[35] H. Bonnemann, W. Brijoux, A. Schulze Tilling, K. Siepen, Top. Catal. 4 (1997) 217.
[36] R.N. Lacey, Patent 888,999, 1960.
[37] M.P.R. Spee, D.M. Grove, G. van Koten, J.W. Geus, in: H.U. Blaser, A. Baiker, R. Prins (Eds.), Heterogeneous Catalysis and Fine Chemicals, vol. IV, Elsevier, New York, 1997, p. 313.
[38] T.M. Dukhovnaya, K.K. Dzhardamalieva, D.T. Nigmetova, D.V. Sokolskii, Rus. J. Phys. Chem. 57 (1983) 373.
[39] H. Hoffmann, G. Boettger, K. Baer, H. Wache, H. Graefje, W. Koernig, US patent 4,001,344, 1977.
[40] L.M. Bronstein, D.M. Chernyshov, I.O. Volkov, M.G. Ezernitskaya, P.M. Valetsky, V.G. Matveeva, E.M. Sulman, J. Catal. 196 (2000) 302.
[41] D.V. Sokol'skii, N.V. Anisimova, A.K. Zharmagambetova, L.M. Kurashvili, L.N. Edygenova, Rus. J. Phys. Chem. 60 (1986) 1639.
[42] G.D. Zakumbaeva, N.A. Zakarina, N.F. Toktabaeva, A.V. Ermolaev, L.N. Abramov, Rus. J. Appl. Chem. 54 (1981) 980.
[43] BASF, GB patent 871,804, 1961.
[44] R.V. Chaudhari, M.G. Parande, P.A. Ramachandran, P.H. Brahme, H.G. Vagaonkar, R. Jaganathan, AIChE J. 31 (1985) 1891.
[45] T.A. Nijhuis, G. van Koten, F. Kaptejn, J.A. Moulijn, Catal. Today 79–80 (2003) 315.
[46] J. Yu, J.B. Spencer, Chem. Comm. (1998) 1103.
[47] J.M. Winterbottom, H. Marwan, J. Viladevall, S. Sharma, S. Raymahasay, in: H.U. Blaser, A. Baiker, R. Prins (Eds.), Heterogeneous Catalysis and Fine Chemicals, vol. IV, Elsevier, New York, 1997, p. 59.
[48] R. Tschan, M.M. Schubert, A. Baiker, W. Bonrath, L.H. Rotgerink, Catal. Lett. 75 (2001) 31.
[49] B. Coq, F. Figueras, J. Mol. Catal. A 173 (2001) 117.
[50] C. Badini, F. Laurella, Surf. Coat. Tech. 135 (1991) 291.
[51] K.S. Lee, K.H. Oh, W.W. Park, H.Y. Ra, Scripta Mater. 39 (1998) 1151.
[52] Y. Ohya, T. Kume, T. Ban, Jpn. J. Appl. Phys. 44 (2005) 1919.
[53] Y. Ohya, T. Ogata, T. Ban, Y. Takahashi, J. Cerym. Soc. Jpn. 113 (2005) 220.
[54] Y. Ohya, M. Ueda, Y. Takahashi, Jpn. J. Appl. Phys. (1996) 4738.
[55] Y. Ohya, T. Niwa, T. Ban, T. Takahashi, Jpn. J. Appl. Phys. 40 (2001) 297.
[56] G.M. Maksimov, K.I. Matveev, V.I. Zajkovskij, N.A. Zakarina, I.F. Toktabaeva, G.D. Zakumbaeva, SU patent 1420714 A1, 1995.
[57] D. Dollimore, G.R. Heal, J. Appl. Chem. USSR 14 (1964) 109.
[58] M. Valentini, G. Groppi, C. Cristiani, M. Levi, E. Tronconi, P. Forzatti, Catal. Today 69 (2001) 307.
[59] J. Haber, Pure Appl. Chem. 63 (1991) 1227.
[60] N. Iwasa, M. Yoshikawa, M. Arai, Phys. Chem. Chem. Phys. 4 (2002) 5414.
[61] T. Takequchi, Y. Kani, M. Inoue, K. Eguchi, Catal. Lett. 83 (2002) 49.
[62] S. Liu, B. Yue, K. Jiao, Y. Zhou, H. He, Mater. Lett. 60 (2006) 154.
[63] C.-T. Hong, C.-T. Yeh, F.-H. Yu, Appl. Catal. 48 (1989) 385.
[64] G.D. Zakumbaeva, V.A. Naidin, T.S. Dagirov, E.N. Litvyakova, Rus. J. Phys. Chem. 61 (1987) 801.
[65] N. Iwasa, S. Masuda, N. Ogawa, N. Takezawa, Appl. Catal. A 125 (1995) 145.
[66] N. Iwasa, T. Mayanagi, W. Nomura, M. Arai, N. Takezawa, Appl. Catal. A 248 (2003) 153.
[67] A. Sarkany, Z. Zsoldos, B. Furlong, J.W. Hightower, L. Guczi, J. Catal. 141 (1993) 566.
[68] N. Semagina, A. Renken, D. Laub, L. Kiwi-Minsker, J. Catal. 246 (2007) 308.
[69] S. Leviness, V. Nair, A.H. Weiss, Z. Schay, L. Guczi, J. Mol. Catal. 25 (1984) 131.
[70] M.A.S. Baldanza, L.F. de Mello, A. Vannice, F.B. Noronha, M. Schmal, J. Catal. 192 (2000) 64.
[71] U.K. Singh, M.A. Vannice, J. Catal. 191 (2000) 165.

[72] J.A. Alves, S.P. Bressa, O.M. Martinez, G.F. Baretto, Chem. Eng. J. 125 (2007) 131.
[73] R.I. Macey, G.F. Oster, Berkeley Madonna (1997).
[74] M.A. Aramendia, V. Borau, C. Jimenez, J.M. Marinas, M.E. Sempere, F.J. Urbano, Appl. Catal. 63 (1990) 375.
[75] J.P. Boitiaux, J. Cosyns, S. Vasudevan, Appl. Catal. 15 (1985) 317.
[76] J. Rajaram, A.P.S. Narula, H.P.S. Chawla, S. Dev, Tetrahedron 39 (1983) 2315.
[77] M.G. Sulman, Rus. Chem. Rev. 69 (2000) 165.
[78] J.-P. Mikkola, T. Salmi, Chem. Eng. Sci. 54 (1999) 1583.